NEW FINE-SCALE INVESTIGATION OF IRREGULAR MARE PATCHES. G. M. Wolff[1,2], J. D. Stopar[1], E. G. Rivera-Valentín[1,3], L. Jozwiak[3], G. Morgan[4], A. M. Bramson[5], A. Virkki[6] [1]Lunar and Planetary Institute (USRA), Houston, TX; [2]University of Colorado, Colorado Springs, CO; [3]JHU-Applied Physics Laboratory, Laurel, MD; [4]Planetary Science Institute, Washington, DC; [5]Purdue University, West Lafayette, IN; [6]University of Helsinki, Helsinki, Finland.

Introduction: Irregular Mare Patches (IMPs) are potentially young (<100 Ma) features notable for their unique bulbous mounds with uniform surface texture and topographically uneven deposits [e.g., 1–5]. IMPs occur at volcanic shields/domes, mare rilles, and within mare plains [4]. Determining their ages and formation is critically tied to constraining models of lunar thermal evolution and identifying volcanic or geomorphologic processes on the Moon. Proposed formation mechanisms include lava lakes, inflated lava flows, magmatic foam/lava extrusions, volatile outgassing, and regolith drainage [list in 6]. To further characterize IMPs, we combined Lunar and Reconnaissance Orbiter (LRO) Mini-RF data, including new collects acquired since [7], with other data sets to further analyze their features.

Methods: Mini-RF S-band (12.6 cm) monostatic collects cover large portions of the Ina, Cauchy, Hyginus, and Sosigenes Crater IMPs and their surroundings, and one bistatic S-band collect covers the Cauchy IMP. Stokes parameters (S1–S4), same-sense circular polarization (SC), opposite-sense circular polarization (OC), and circular polarization ratio (CPR = SC/OC) products were used in this study. Surface roughness relative to wavelength can be inferred from radar and has been used to distinguish variations between different types and ages of lava flows on Earth [8–10] and analyze impact melts on the Moon [11]. The radar data are sensitive to ~1–2 m depths, related to Fe,Ti content [12]. We also performed m-Chi decompositions [13] to create RGB images depicting the type of polarization returned from each pixel (single-bounce=blue, randomly polarized or volume scattering=green, and double-bounce=red). Calibrated, high-resolution Lunar Reconnaissance Orbiter Camera (LROC) NAC images and 2 or 5 m digital elevation models (DEMs) [14, 15] provided comparisons, along with multispectral basemaps from LRO, Clementine, and Kaguya/SELENE.

Results: In total backscatter (S1) and m-Chi images, terranes such as mare, highlands, pyroclastic deposits, and impact ejecta were distinguishable through differences in homogeneity, brightness, and average color (i.e., predominantly blue, purple, or yellow). CPR, an indicator of roughness, had a high degree of noise and sensitivity to topography. Ratioing samples of OC and SC values, an alternative to CPR, for different units within the same radar collect revealed differences in range, mean, and trend slope of the ratios. These differences are likely related to particle shapes, composition, ~10-cm scale roughness, and/or topography [16]. Based on the observed characteristics, we identified four general units associated with IMP features: mounds, radar-dark uneven units, radar-bright uneven units, and rocky units (**Fig. 1**).

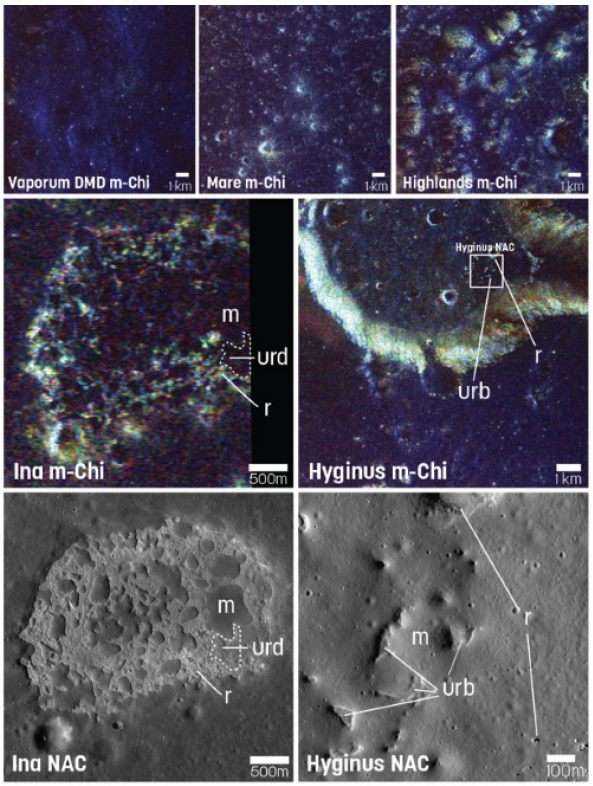

Fig. 1. m-Chi of pyroclastics (Vaporum), typical mare, normal highlands, Ina, and Hyginus. NAC images of Ina and Hyginus IMPs. Examples of radar units marked: mound (m), uneven radar-dark (urd), uneven radar-bright (urb), rocky (r).

Rocky units: Rocky units with numerous exposed rocks evident in NAC imagery are associated with higher S1 and are characterized by an intense multicolored appearance in m-Chi, the result of a high number of wavelength-scale facets with complicated geometries. These are distributed primarily around cliffs (such as the outer portions of the Ina depression; **Fig. 1**), impact craters, and uneven units.

Radar-bright uneven units: Many uneven patches are radar bright without the presence of rocks in NAC imagery. This could result from the presence of rocks smaller than image resolution, buried rocks, a consolidated material, or complex regolith grain properties within the upper meters. These materials are

multicolored in the m-Chi, consistent with an uneven texture creating similarly complicated geometries. OC and SC trends for these units are more like that of crater ejecta than pyroclastics, mare, or highlands.

Mounds and radar-dark uneven units: In all studied IMPs, portions of mounds and uneven units have low backscatter returns (**Fig. 1**). Eastern slopes on mounds are dominated by blue in the m-Chi, consistent with a spacecraft-facing slope of material that is smooth at wavelength scales. Observed OC and SC trends are similar to "typical" mare or pyroclastic deposits.

Discussion of Ina: Ina's center has low radar backscatter, with portions of both the mounds and uneven deposits nearly indistinguishable. Thus, we believe a rock-poor material of at least 1–2 m to be present in the areas within Ina not dominated by rocks. Superposed craters on mounds without the presence of excavated rocks indicates this depth may extend further. This agrees with analyses of DFSAR L-band radar [Bhiravarasu et al., this conference] and Diviner data that predicts at least 15 cm of regolith (or fine-grained material) is present in areas of low thermal inertia (high H-parameter) [6, 17]. These data may support a connection between the presence of smooth pyroclastic deposits and IMPs; however, hyperspectral Moon Mineralogy Mapper data only indicates abundant volcanic glass (e.g., pyroclastic) exterior to Hyginus, with only minor amounts in Ina, Cauchy, and other IMPs [18].

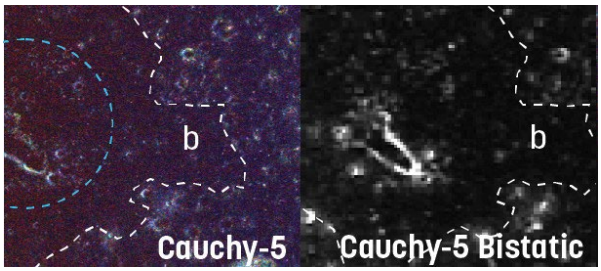

Fig. 2. M-chi and S1 Mini-RF image with radar-dark materials outlined in white dashes; Cauchy shield outline in blue dashes; b=lobate extension. Image width ~ 1.7 kilometers.

Discussion of Other IMPs: Radar dark uneven units are also present at Cauchy and Sosigenes Graben (visible in x-band data). Radar bright units are small, separated spots that occur within Hyginus, Sosigenes Crater, and outside the central depression of Cauchy. If present in Ina, they are obscured by the presence of rocks.

Relatively dark, blue/purple, and homogenous areas in m-Chi products surrounding Hyginus and Cauchy indicate the presence of fine-grained, rock-poor material (**Figs. 1&2**), potentially consistent with pyroclastics [7]. This material exhibits a lobate, flow-like extension visible in both the m-Chi and the bistatic collect of Cauchy. These areas share radar characteristics with dark mantling deposits near Mare Vaporum [19]. The exteriors of Ina and Sosigenes Crater, on the other hand, are indistinguishable in radar from other mare and highlands terrain. If pyroclastic material is present in these areas, then it is not easily discernable.

Conclusions: The association of radar-dark units with both mound and uneven units is consistent with abundant, meters-thick, fine-grained, and rock-poor surface materials. These deposits at Ina and several other IMPs suggests several possibilities: there are significant pyroclastic deposits ranging from scoria to ash (e.g., mildly explosive phases of the eruption); a fine particulate surface on top of a lava flow [20]; or these are old volcanic deposits that have developed a meters thick regolith. If the IMP features are primarily volcanic in origin, they must have remarkably low abundances of iron-bearing glass [18].

Acknowledgments: Data were acquired from the LRO Mini-RF and LROC teams, the NASA PDS archive, and the JAXA archive. All utilized data are publicly hosted in NASA's PDS archive or the JAXA archive. This work was funded by the LPI Summer Intern Program in Planetary Science, the Lunar Reconnaissance Orbiter Mini-RF and LROC Teams, and an LDAP Grant (PI J. Stopar).

References: [1] Strain and El-Baz (1980) *Proc. Lunar Planet. Sci. Conf. 11th*, p. 2437–2446. [2] Schultz et al. (2006) *Nature*, 444(7116), 184–186. [3] Stooke (2012) *JGR*, 125, 10.1029/2019JE006362. [4] Braden et al. (2014) *Nature Geoscience*, 10.1038/NGEO2252. [5] Qiao et al. (2019) *JGR*, 124 1100–1140. [6] Byron et al. (2022) *JGR*, 127. [7] Carter et al. (2013) *LPSC*, 2146. [8] Mazzarini et al. (2007) 10.1029/2005JB004166. [9] Gaddis et al. (1990) *Photogrammetric Engineering & Remote Sensing,* Vol. 56. [10] Whelley et al. (2017) *Bull. Volcanol.*, 10.1007/s00445-017-1161-5. [11] Neish et al. (2017) *Icarus*, 10.1016/j.icarus.2016.08.008. [12] Fa et al. (2011) *JGR*, 116, 10.1029/2010JE003649. [13] Raney et al. (2012) *JGR*, 117, 10.1029/2011JE003986. [14] Robinson et. al. (2010), *SSR,* Vol 150, pp. 81–124. [15] Henriksen et al. (2017) *Icarus*, 283: 122–137. [16] Virkki and Bhiravarasu (2019) *JGR*, 124, 10.1029/2019JE006006. [17] Elder et al. (2017) *Icarus,* 290, 224–237. [18] Vannier et al. (2022) *LPSC,* 2311. [19] Weitz et al. (2021) *LPSC,* 7011. [20] Qiao et al. (2020) *JGR-Planets*, 10.1029/2019JE006362. [21] Carrier et al. (1991) *Cambridge Univ. Press, New York*, 475–594. [22] Garry et al. (2012) *JGR*, 117, 10.1029/2011JE003981. [23] Stopar et al. (2019) *PSS,* 171, 1–16. [24] Qiao et al. (2021) *PSJ,* 2:66, 10.3847/PSJ/abeaa0. [25] QuickMap Tool: https://quickmap.lroc.asu.edu.